ELSEVIER

Polymer 44 (2003) 1459–1467

polymer

www.elsevier.com/locate/polymer

Competition between microphase separation and crystallization in self-assembly sPS/PS-PEP blends

Rong-Ming Ho[a,*], Chun-Cheng Chang[b], Tsai-Ming Chung[b], Yeo-Wan Chiang[b], Jeng-Yue Wu[b]

[a]*Department of Chemical Engineering, National Tsing Hua University, Hsinchu 30013, Taiwan, ROC*
[b]*Department of Chemical Engineering, National Chung-Hsing University, Taichung 40227, Taiwan, ROC*

Received 14 October 2002; received in revised form 18 December 2002; accepted 20 December 2002

Abstract

The crystallization and the self-assembly of blending system, syndiotactic polystyrene/polystyrene-*block*-poly(ethylenepropylene) (sPS/PS-PEP), were investigated by transmission electron microscopy (TEM), polarized light microscopy, small angle X-ray scattering and differential scanning calorimetry (DSC). Spherical microdomains with sPS embedded in PS-PEP matrix were obtained after melt mixing as evidenced by TEM observations combined with DSC analyses. The size of spherical microdomains is in the order of tens nanometer. This unique morphology provides an appropriate system to examine the effect of crystallization on microphase-separated morphology. The driving force of sPS crystallization leads the growth of sPS crystals to overcome the effect of spatial confinement and the repulsive barrier of immiscibility, and thus to go across the surrounding PEP domains. As a result, the growth of crystallization interconnects sPS microdomains and forms crystalline lamellae. The overall crystallization rate of sPS in self-assembly sPS/PS-PEP blends increases with increasing the content of sPS. We suggest that the increase on the crystallization rate is attributed to the decrease on the crossing-distance between the crystallizing sPS domains due to an increase on the size of spherical microdomain.

Keywords: Syndiotactic polystyrene; Polystyrene-*block*-poly(ethylenepropylene); Confinement

1. Introduction

The self-assembly microstructures of block copolymers driven by immiscibility between their constituted blocks have attracted extensive studies because of the formation of nano-scale microstructures that appears promising in the applications of nano-technology such as ultra-filtration membrane, nanopatterned template, nano-reactor matrix, nano-device etc. [1–5]. The majority of these studies focus on the phase behavior of amorphous block copolymers at which the nano-scale microstructure is formed by balancing interfacial energy and entropic penalty such as chain stretching and localization of chemical connection to minimize the Gibbs free energy of final morphology and to maintain mean density [6–10]. More recently, the studies on the crystalline morphology for crystallizable block copolymers have become another important aspect to the applications of block copolymer microstructures. The formation of crystalline domains within microphase-separated morphology gives rise to another dimension for considering the physical and mechanical properties of ordered microstructures. It has been found that the final morphology of crystallizable block copolymers is strongly dependent upon the comparative temperatures of order–disorder transition temperature (T_{ODT}), crystallization temperature of crystallizing blocks (T_c) and glass transition of amorphous blocks ($T_{g,A}$) as well as crystallization rate [11–22]. In other words, the formation of crystallized morphology is the consequence of the competition between the driving forces of crystallization, vitrification and microphase separation.

To understand the effects of crystallization on microphase-separated textures is critical for the applications of crystallizable block copolymers in nano-technology. It is generally agreed that the final morphology is driven by the crystallization of crystallizable blocks regardless of the microphase separation of block copolymers when T_c is above T_{ODT} and $T_{g,A}$. For systems with $T_{ODT} > T_c \geq T_{g,A}$ (i.e. a soft confinement for crystallization), the

* Corresponding author. Tel.: +886-3-5738349; fax: +886-3-5715408.
E-mail address: rmho@mx.nthu.edu.tw (R.M. Ho).

0032-3861/03/$ - see front matter © 2003 Elsevier Science Ltd. All rights reserved.
doi:10.1016/S0032-3861(03)00012-0

microphase-separated morphology may be destroyed by the effect of crystallization. In contrast to the soft confinement, the microstructure preserves if $T_{ODT} \gg T_{g,A} > T_c$ (i.e. a hard confinement for crystallization) [23–25]. The occurrence of microstructure destruction after crystallization is also governed by the mobility of copolymer chains where the chemical connection between crystallizable and amorphous blocks might affect the chain mobility. Recently, the mutual interaction between the effect of segregation strength (i.e. the product of molecular weight of block copolymer and incompatibility between constituted block) and crystallization on block copolymer morphology has also been systematically studied by Register and co-workers [26]. As described, the block copolymer microstructure by microphase separation maintains regardless of the mobility effect on crystallization while the segregation strength is strong enough. As a result, the final morphology of crystallizable block copolymers involves many dependent factors such as molecular weight, immiscibility between constituted blocks, composition, glass transition temperature of amorphous block, crystallization window of crystallizable block and so on.

In this study, we are interested in the crystallization effect on the final morphology of self-assembly sPS/PS-PEP blends. We simply melt mixed syndiotactic polystyrene (sPS) with commercial styrenic diblock copolymer, polystyrene-*block*-(polyethylenepropylene) (PS-PEP). Spherical microdomain texture with sPS embedded in PS-PEP matrix was obtained. Since the crystallizable chain is not chemically connected to the amorphous microstructure, we name this self-assembly morphology as physically confined system for crystalline polymer so as to distinguish traditional crystallizable block copolymers where the crystallizable block is chemically connected by amorphous block (referred as chemically confined system in this study) [27]. This unique morphology having crystallizable sPS component localized inside the shell of PS-rich domain gives rise to a specific crystallization environment where the crystallization of crystallizable blocks is carried out from nano-scale microdomains without the restrain of chemical connection. Having these blending microstructures allows us to achieve understanding of crystallization mechanism from nano-scale microdomains without the effect of chemical connection.

2. Experimental

2.1. Materials

Semicrystalline syndiotactic polystyrene was synthesized in terms of the metallocene polymerization of styrene catalyzed by a typical aluminum alkoxide at Union Chemical Laboratories, Industrial Technology Research Institute (ITRI). Detailed synthetic routes are similar to the procedure described by Chien and Salajka [28]. The number-averaged molecular weight of the samples is 25,000 g/mol and the polydispersity is 2.6 based on the measurement of high-temperature size exclusion chromatography (SEC). The styrenic block copolymer used in this investigation is a diblock copolymer of polystyrene-*block*-poly(ethylenepropylene) symbolized as PS-PEP (Kraton G1702 of Shell Co.). According to the supplier, this commercial PS-PEP possesses 28 wt% styrene content. SEC result indicated that the number-averaged molecular weight, M_n, of as-supplied PS-PEP is 175,000 g/mol and a polydispersity index is 1.12.

2.2. Blending processes

Melt-mixed samples were prepared in a MiniMax mixer. The MiniMax mixing cup was preheated to 280 °C, and the pre-mixed blends were simultaneously introduced. Each blend was melt processed at 280 °C for 20 min at 400 rpm. The mixer was purged with industrial grade nitrogen gas before loading to reduce degradation; blending was done under a nitrogen blanket. During mixing, the rotor plate was raised intermittently every several minutes to promote more efficient mixing. After processing, the samples were quenched by ice water. It is noted that there is no significant change in the molecular weight of the PS-PEP for these melt-mixed samples after processing as evidenced by SEC measurements. This result suggests that degradation of PS-PEP during processing is a minor effect. In contrast to PS-PEP, the sPS is basically more stable than PS-PEP.

2.3. Microscopy

Thin films of bulk blending samples having thickness of micrometer range and of tens of nanometer for polarized light microscopy (PLM) and transmission electron microscopy (TEM) observations, respectively, were obtained by ultra-cryomicrotomy using a Reichert Ultracut microtome (equipped with a Reichert FCS cryochamber and a diamond knife). All of the samples prepared by cryomicrotomy were operated at −120 °C. PLM image was obtained by an OLYMPUS BX60 PLM installed with a DP10 digital camera. Bright field mass-thickness contrast TEM images of stained samples were obtained by a JEOL JEM-1200x TEM, at an accelerating voltage of 120 kV. Staining was accomplished by exposure the samples to the vapor of a 4% aqueous RuO_4 solution for 30 min.

2.4. Small angle X-ray scattering (SAXS)

SAXS experiments were conducted at the synchrotron X-ray beam-line X27C at the National Synchrotron Light Source in Brookhaven National Laboratory. The wavelength of the X-ray beam is 0.1307 nm. The zero pixel of the SAXS patter was calibrated using a duck tendon and scattering vector $q(q = 4\pi\lambda^{-1} \sin\theta$, where λ is the

wavelength of synchrotron radiation, 2θ is the scattering angle) was determined with silver behenate.

2.5. Differential scanning calorimetry (DSC)

DSC experiments were carried out in a Perkin–Elmer DSC 7. The temperature and heat flow scales were carefully calibrated using standard materials. The samples were first heated to 290 °C, the maximum annealing temperature, T_{max}, for 5 min in order to eliminate the crystalline residues formed during the preparation procedure. The polymer samples were then cooled at a rate of 150 °C/min to generate amorphous glassy samples or to a preset temperature, T_c, for isothermal crystallization. Consecutive heating was performed at heating rates of 10 °C/min. For the melting and crystallization experiments, the DSC sample size was around five milligrams for all the studies.

For the T_g measurements of PS-rich phase and the sPS, the DSC sample size was more than 15 mg. The temperature dependence of heat capacity for polymer samples was thus determined according to the execution of blank, calibration and sample runs based on the standard procedure described in the textbook of thermal analysis by Wunderlich [29]. A heating rate of 10 °C/min was used for all the measurements. On the basis of thermodynamics, the glass transition was defined as an apparent second-order transition. Glass transition temperatures of this study were measured as the 50% change of the heat capacity in the range of glass transition [29].

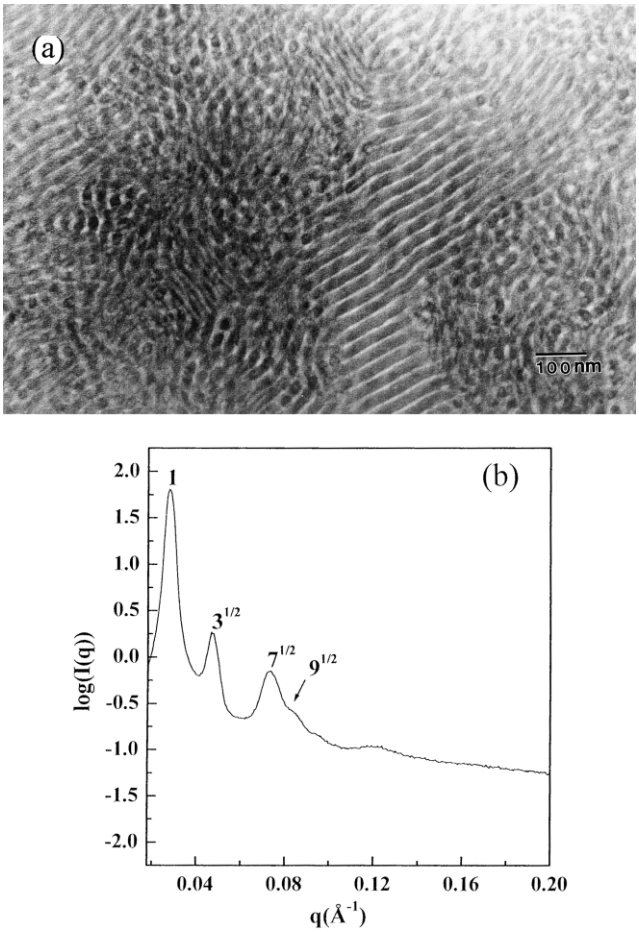

Fig. 1. (a) TEM micrograph of micro-sectioned PS-PEP by mass-thickness contrast. (b) One-dimensional (1D) SAXS profiles of PS-PEP.

3. Results and discussion

3.1. Morphology of sPS/PS-PEP blends

The morphology of PS-PEP microstructure after melt processing is shown in Fig. 1a. The morphological observation demonstrates that the block copolymer of PS-PEP self-assembles to form hexagonal cylinder (HC) microstructure. The microdomains of PS component appear relatively dark after staining by RuO_4, while the microdomains of PEP component appear light. The corresponding SAXS result further confirms the observed texture where the diffraction peaks occurs at relative $q^*(q = 4\pi\lambda^{-1} \sin\theta$, where λ is the wavelength of synchrotron radiation and 2θ is the scattering angle) values of $1{:}3^{1/2}{:}7^{1/2}{:}9^{1/2}$ (Fig. 1b). The long period for the inter-cylinder spacing is determined as 22.7 nm. Micellization was observed while various amounts of sPS (i.e. 15, 30 and 50 wt%) were introduced to the matrix of PS-PEP. Macrophase-separated (i.e. above sub-micrometer size) domains have not been observed even at 50 wt% added amount of homopolymer sPS. It is also noted that all the blends studied appear optically transparent after quenching from amorphous self-assembly microstructure. The results implicitly indicate that the occurrence of macrophase separation (i.e. the size of dispersed domain is larger than sub-micrometer) in the blending samples does not exist. As shown in TEM micrographs of Fig. 2, the morphology texture of melt-mixed sPS/PS-PEP blends exhibits a spherical microdomain texture where the gray spherical microdomain are dispersed in the light matrix. We suggest that the gray domains correspond to amorphous sPS-rich and PS-rich phases and the light domains is the PEP phase. At lower sPS content such as blends with 15 wt% sPS content (Fig. 2a), the formation of spherical microdomain is homogeneously distributed within the matrix of HC morphology. Further increasing the sPS content in blends leads to an overall transformation from the original HC microstructure of PS-PEP to the spherical microdomain texture of sPS/PS-PEP (for instance, the blends with 30 wt% sPS as shown in Fig. 2b). On the assumption of uniform microdomain particle size in blends, the averaged domain size of the micelle is around 50–60 nm in diameter for blends having 15 and 30 wt% sPS contents as estimated from over one hundred micelle particles. Larger spherical microdomain (about 70–90 nm in diameter) was found while larger amount of sPS was introduced as illustrated in Fig. 2c for the blends with 50 wt% sPS. The corresponding SAXS experiments for the sPS/PS-PEP

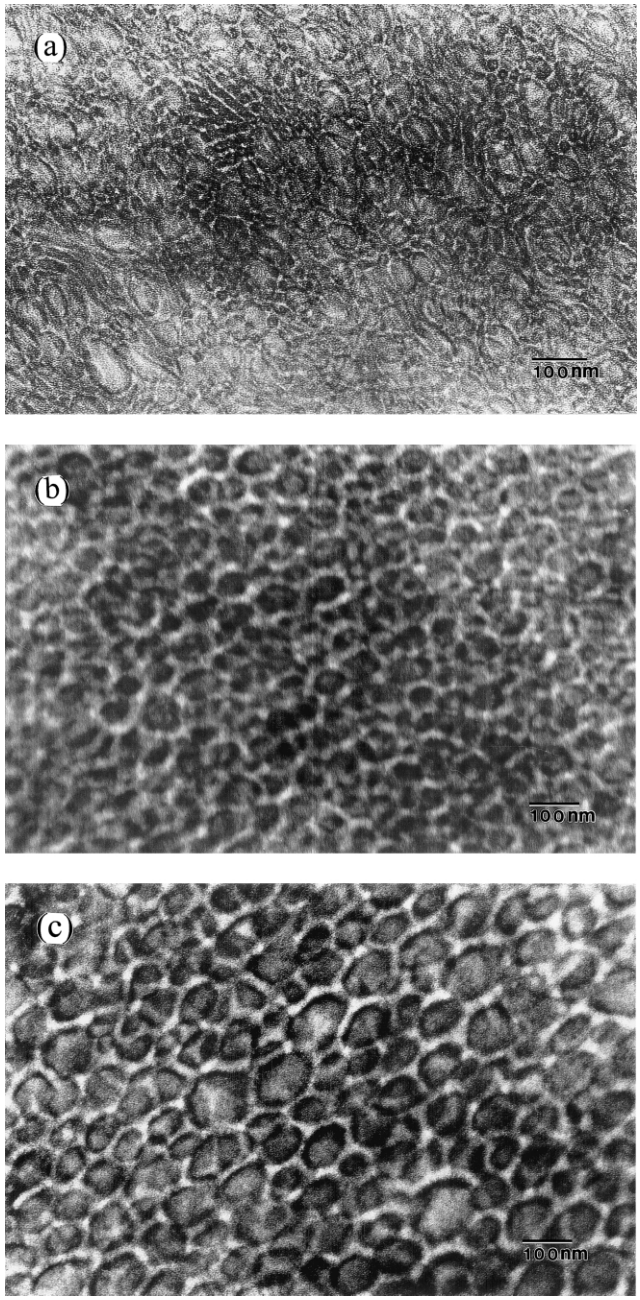

Fig. 2. TEM micrographs of micro-sectioned sPS/PS-PEP blends having (a) 15 wt%; (b) 30 wt%; (c) 50 wt% sPS content by mass-thickness contrast.

blends were also carried out in order to identify the observed TEM morphology so as to determine the inter-distance between the spherical microdomains. However, no significant diffraction result was obtained. To further confirm the formation of spherical microdomain texture, tilting experiments by TEM were carried out to construct the microstructure from different projection images. Spherical morphology was clearly identified at different projections.

3.2. Behavior of micellization

Since the occurrence of macrophase separation is absent in the sPS/PS-PEP blends, we thus deduce that the sPS component is either located in the core of formed spherical microdomain or mixed with PS block as illustrated in Fig. 3a and b, respectively. The first instance was designated by Hashimoto and coworkers as the behavior of localization for a homopolymer blended in a block copolymer, whereas the later instance the behavior of solubilization [30,31]. To further identify the formed texture of sPS/PS-PEP, the blends were examined by DSC. The T_g temperature of sPS samples was determined as 90.6 °C (Fig. 4a) whereas the T_g temperature of PS-rich phase in the PS-PEP copolymer was determined as 98.4 °C (Fig. 4b). Fig. 5 shows the DSC thermograms of various sPS/PS-PEP blends. The T_g of sPS-rich phase in the blends is in the vicinity of 91 °C (Fig. 5) that is almost equal to the T_g of homopolymer sPS. However, the T_g transition of PS-rich phase becomes non-recognizable for the melt-blended samples. According to the enthalpic interaction between constituted components in the blends, it is reasonable to presume that the sPS component is of favor PS blocks instead of PEP blocks. Solubilization of sPS into PS blocks inevitably brings the T_g transitions of the PS and the sPS closer to each other, and thus, leads to the transformation of cylindrical microstructure to lamellar morphology as shown in Fig. 3b. In fact, the change on the T_g of the sPS in blends has not been found, and the microstructure transformation does not occur. Furthermore, only if the PS blocks adopt almost extended chain conformation, and then it is possible to have such large size of spherical microdomain (above 50 nm) when the solubilization behavior completely dominates. We thus deduced that the majority of sPS is localized and embedded in the microdomains of PS block; the behavior of localization for the sPS dominates the behavior of solubilization. However, there is still certain amount of sPS solubilized into the PS domains so that the PS-rich phase forms a PS concentration profile and thus exhibits invisible T_g transition. As a result, we conclude that the majority of sPS component is localized inside the micro-damains of PS-rich phase.

The next question is that what is the origin to form the spherical morphology as illustrated in Fig. 3c instead of typical texture for localization as shown in Fig. 3a. One of the possible interpretations for the formation of this unique microstructure is ascribed to the result of processing effect. To alleviate the influence of processing, melt-blending amorphous samples were further annealed at T_{max} for one day. No significant change on the morphology of sPS/PS-PEP blends was observed after annealing expect for the formation of certain larger spherical microdomains. As a result, we hypothesize that the occurrence of spherical microstructure must be in relevant to the thermodynamic origin. According to the thermodynamics of mixing, the blending system of sPS/PS-PEP is similar to the ordinary A/A–B blends where a small negative value of interaction parameter between sPS and PS has been identified [32]. Our previous studies have found that macrophase separation for

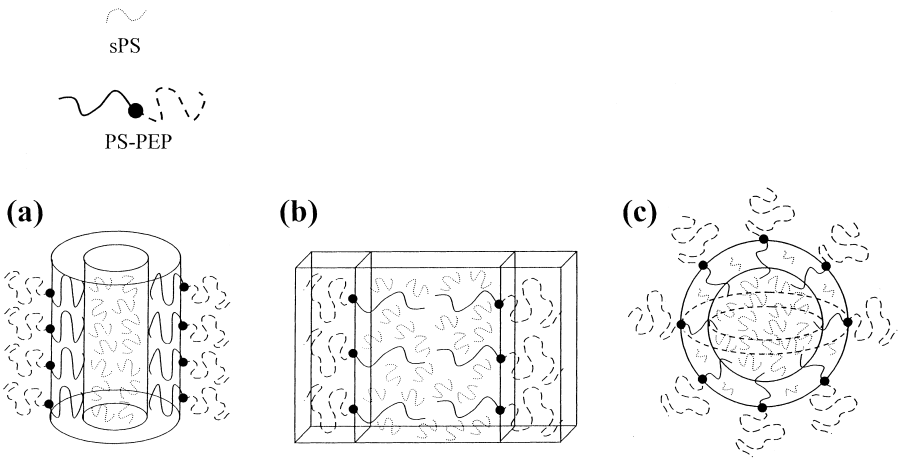

Fig. 3. Schematic diagrams of the behavior of (a) the localization; (b) the solubilization; (c) the proposed morphology for sPS in PS-PEP block copolymer matrix.

sPS/styrenic block copolymer blends occurs while the ratio of the number-averaged molecular weight of sPS ($M_{n,sPS}$) to the PS block of copolymer ($M_{n,PS}$) is larger than one [33]. This result is consistent with the phase behavior of the ordinary A/A–B blends [34–44]. For the formation of sPS spherical microdomain in sPS/PS-PEP blends, we speculate that the specific microstructure is attributed to the broad molecular weight distribution of sPS. Although the ratio of number-averaged molecular weights for sPS and PS block ($M_{n,sPS}/M_{n,PS}$ = 25,000/49,000 ~0.51) is smaller than one, the ratio of the weight-averaged molecular weight of sPS to the number-averaged molecular weight of PS block ($M_{w,sPS}/M_{n,PS}$ = 62,500/49,000 ~1.28) is larger than one. For the polydispersity of 2.6, it is possible to exhibit the behavior of solubilization (i.e. $M_{sPS}/M_{PS} < 1$), localization (i.e. $M_{sPS}/M_{PS} \sim 1$) and macrophase separation (i.e. $M_{sPS}/M_{PS} > 1$) at once for the sPS/PS-PEP blends on the basis of thermodynamic consideration for the ordinary A/A–B blends. As a result, we speculate that the fractions of low molecular weight sPS work as surfactant so as to create the shells of spherical microdomains. The fractions of high molecular weight form phase-separated microdomains having limitation in size due to the effect of compatibilization. Combining with the possible formation of solubilized sPS into PS-rich domains, preferentially localized sPS within PS-rich domains and sPS macrophase separation, spherical morphology with tens of nanometer size surrounded by PEP was observed. This spherical microdomain possessing the core of localized sPS chains embedded by the shell of PS-rich domains at its lowest Gibbs free energy (i.e. a stable phase in thermodynamics) was formed. Further studies, especially the thermodynamic derivations, are necessary to elucidate the complicated phase behavior of the sPS/PS-PEP blends. Nevertheless, the self-assembly sPS/PS-PEP is indeed to create a three-dimensional confined environment for the studies of sPS crystallization behavior. On the basis of the microstructure identification, the concept of physical confinement can then be applied.

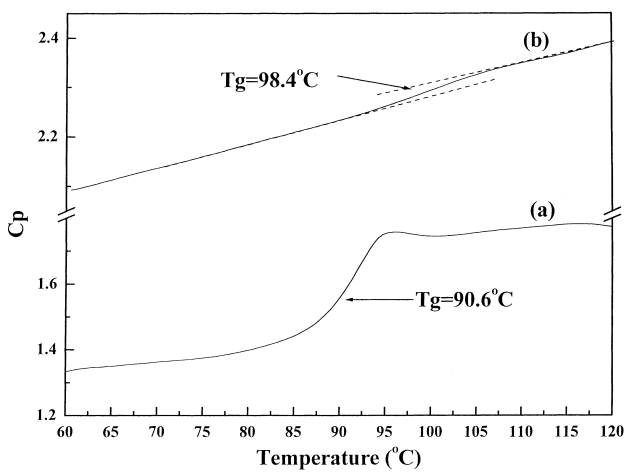

Fig. 4. DSC thermograms of (a) sPS and (b) PS-PEP. The heating rate is 10 °C/min for all the scans.

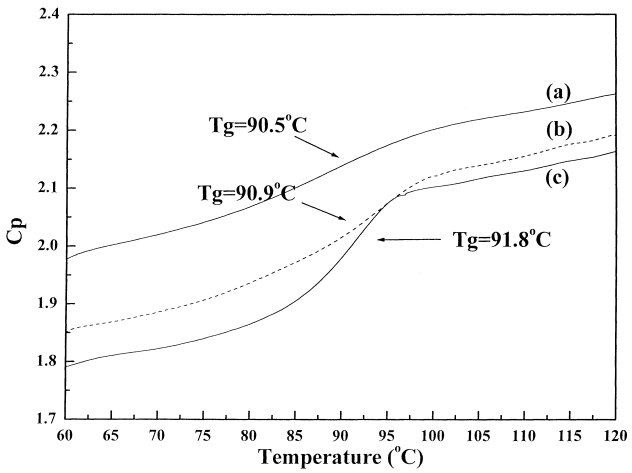

Fig. 5. DSC thermograms of various sPS/PS-PEP blends having (a) 15 wt%; (b) 30 wt%; (c) 50 wt% sPS content. The heating rate is 10 °C/min for all the scans.

3.3. Competition between crystallization and microphase separation

To visualize the crystallization effect on the self-assembly spherical morphology of sPS/PS-PEP blends, the crystallization of the sPS from the core of spherical microdomain was carried out at temperature between melting temperature (ca. 240–270 °C) and glass transition temperature (ca. 100 °C) from the melt ($T_{max} = 290$ °C). It is noted that the T_{max} and the crystallization temperature for the sPS in the blends are below the T_{ODT} of block copolymer PS-PEP ($T_{ODT} > 320$ °C) [45], and much higher than the T_gs of amorphous components. It is also noted that the segregation strength of PS-PEP microphase separation is not strong enough to confine the crystallization due to the relatively high crystallization temperature for sPS. Crystallization effect on the morphology of self-assembly sPS/PS-PEP blends can thus be studied according to the development of crystallization stage. It is well known that the overall crystallization includes the nucleation and the growth processes. To trace this interrelationship at different crystallization stages, the morphologies of sPS crystallized at various isothermal crystallization times were observed by TEM as an example illustrated in Fig. 6. It is noted that the development of crystallization stage is in accordance with the increasing amount of crystallinity (i.e. the heat of fusion as shown in Fig. 7). In the early stage of crystallization (e.g. $t_c = 1 \ll t_f = 100$ min which is the crystallization time for complete crystallization at $T_c = 240$ °C see Fig. 7), no significant change with respect to the spherical morphology is found (Fig. 6a). It reflects that the crystallization does not affect the microphase separated morphology on the stage of primary nucleation. Further increasing the crystallization time, crystalline lamellar texture starts to be observed as illustrated in Fig. 6b ($t_c = 10$ min). These crystalline lamellae can also be identified by PLM observation where the crystallizing sPS component shows typical birefringence characteristics (Fig. 8a). After extensive isothermal crystallization (Fig. 6c), the crystalline lamellae grow to form large crystallites and exhibited interesting morphology under PLM observations. The growing crystals appear crystalline lamellae (Fig. 8b). Similar morphological observation has also been observed for the sPS in various sPS/PS-PEP blends crystallized at different isothermal crystallization temperatures.

Extensive studies with regard to the change on morphology after crystallization for crystallizable block copolymer (i.e. a chemically confined system) have been devoted [13–24]. As suggested, the final morphological texture is dependent upon a variety of factors including thermodynamic consideration such as minimization of Gibbs free energy and kinetic consideration such as

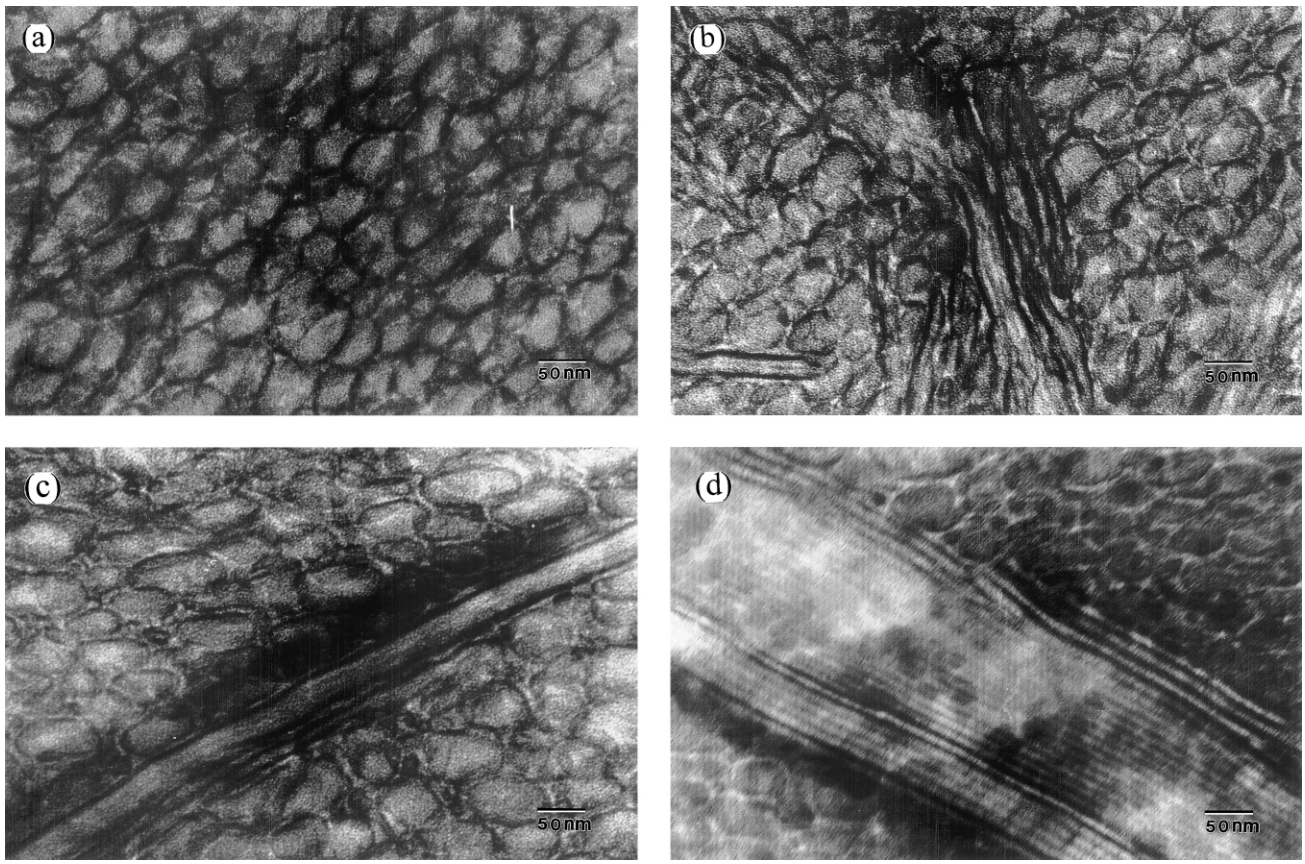

Fig. 6. TEM micrographs of micro-sectioned sPS/PS-PEP blends having 30 wt% sPS content crystallized at 240 °C for (a) 1 min; (b) 10 min; (c) 30 min; (d) 120 min from the melt by mass-thickness contrast.

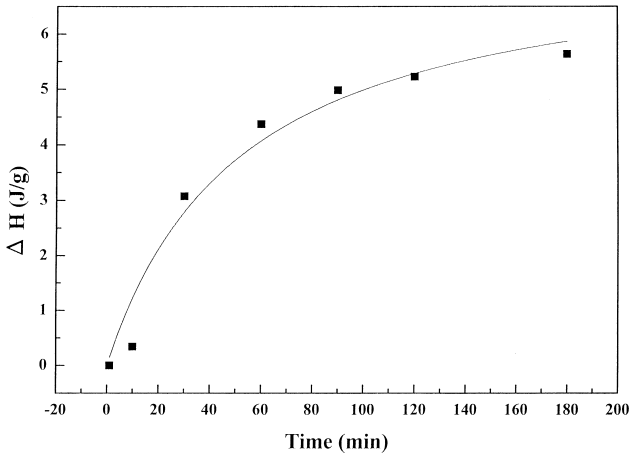

Fig. 7. Plot of endothermic response versus isothermal crystallization time for sPS/PS-PEP blends having 30 wt% sPS content crystallized at 240 °C from the melt.

nucleation and mobility of copolymer chains. For crystallization under soft confinement, the covalent connection between crystallizable and amorphous blocks inevitably influences the final texture of crystallized copolymers since this chemical junction not only affects the Gibbs free energy of final morphology but also determines the mobility of crystallizing blocks. The change on morphology induced by crystallization, particularly the destruction of self-assembly microstructure, is attributed to the thermodynamic driving force of crystallization overcomes the repulsive interaction between constituted blocks and the entropic variation. The entropic variation includes the decreasing on entropy penalty with respect to the arrangement of chemical junction and the stretching chain conformation of amorphous block. On the basis of thermodynamic driving force, the accessibility of morphological change is controlled by the kinetic consideration where the energy barrier of chain mobility plays significant role to decide whether or not the change does occur. In contrast to the chemically confined system, the change on morphology for the sPS/PS-PEP blends is mainly due to the growth of crystallizing sPS of which no covalent connection exists. In other words, the study on the competition between crystallization and microphase separation can be simplified without considering the chemical junction. As a result, the observed morphological development of the crystallized sPS indicates that the driving force of sPS crystallization leads the growth of sPS crystals to overcome the spatially confined effect and the repulsive barrier of immiscibility, and thus to go across the surrounding PEP domain.

To further examine the discussed mechanism, the crystallization rate of the sPS at different isothermal crystallization temperatures was determined on the basis of crystallization exotherm during isothermal crystallization. Usually, the peak time of crystallization, t_p, (i.e. the time taken at the peak of exothermic crystallization) is utilized to be proportional to the reciprocal of crystallization rate of isothermal crystallization. We simply used the peak time as an indication of the crystallization rate. As shown in Fig. 9, the crystallization rate of sPS in the blends is much slower than that of the neat sPS. This reflects that the confinement effect is very critical to the crystallization rate.

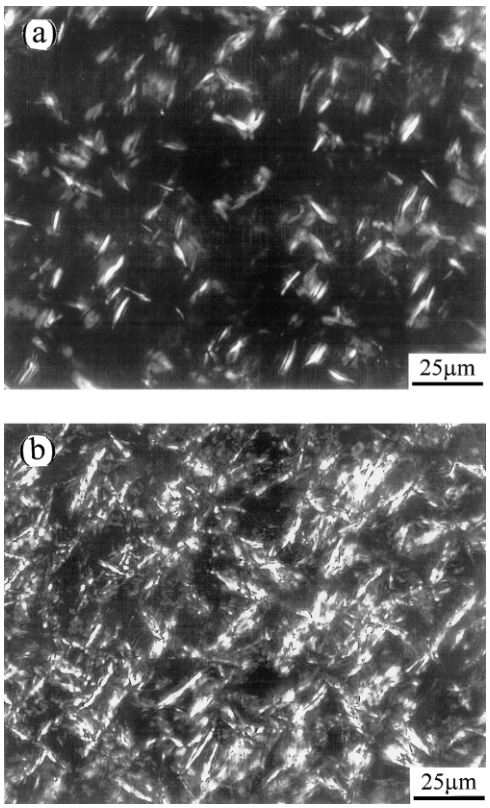

Fig. 8. PLM micrographs of micro-sectioned sPS/PS-PEP blends having 30 wt% sPS content crystallized at 240 °C for (a) 10 min; (b) 120 min from the melt.

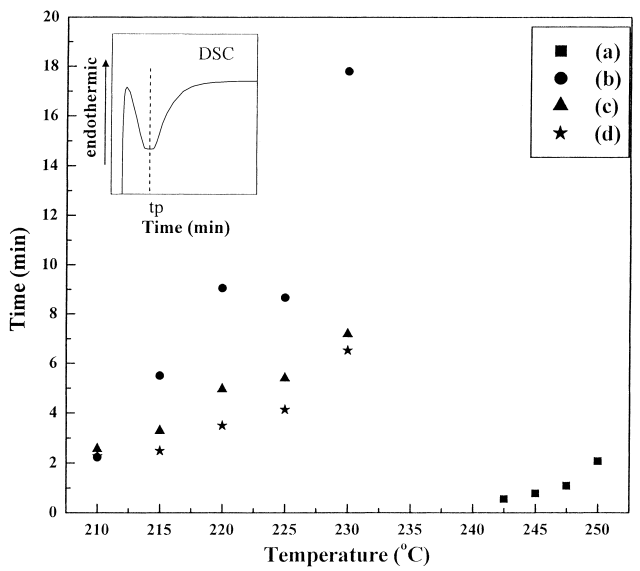

Fig. 9. Crystallization peak times for sPS crystallized at different T_c from the melt of (a) sPS and the sPS/PS-PEP blends having (b) 15 wt%; (c) 30 wt%; (d) 50 wt% sPS content.

However, the crystallization rate of sPS in blends increases with increasing the added amount of sPS in PS-PEP.

Interestingly, the results of crystallization rate correlate with the changes on the self-assembly morphology. For the sPS/PS-PEP blends containing 15 wt% sPS (Fig. 2a), the crossing-distance for crystallized chains going across the PEP domains is much larger than that of the blends having the higher content sPS (Fig. 2b and c) due to the remaining of PS-PEP HC microstructure. In contrast to the sample having 30 wt% sPS, the sample having 50 wt% sPS leads to the formation of larger spherical microdomain size (Fig. 2c) as previously described. In addition to the interface effect of sPS and PS blocks, the energy barrier for sPS crystallization in the self-assembly sPS/PS-PEP blends is thus expected to be strongly dependent upon the changes on crossing-distance and the size of spherical microdomain with increasing the added amounts of sPS (see below for reasons).

3.4. Crystallization mechanism

The mechanism for the sPS crystallization under physical confinement was proposed as the schematic diagram illustrated in Fig. 10. On the stage of primary nucleation, there is no change on the spherical morphology (Fig. 10a). When the crystal growth starts, the spherical microdomain starts to be deformed along the growth direction due to the gradual reduction of amorphous content transverse to the growth direction (Fig. 10b). The growth of crystalline thus breaks out the amorphous PS-PEP boundary and establishes connection to the neighboring spherical microdomains (Fig. 10c). In the meantime, the aggregation of crystalline lamellae may pile up transverse to the growth direction (Fig. 10d). Recently, Register and co-workers reported that the overall crystallization rate for crystallizable block copolymers is strongly dependent upon the volume of the crystallizable microdomains in matrix, particularly in the case of spherical microstructure under hard confinement [46,47]. The smaller the crystallizable microdomains are, the larger the confined effect (i.e. the slower the crystallization rate) can be. Chen and co-workers have also reported similar inferences [48]. For the self-assembly sPS/PS-PEP blends, the spatial effect on sPS crystallization is much more complicated. The miscibility between sPS and PS blocks, in general, decreases the crystallization rate of sPS due to the dilution effect for nucleation. Furthermore, the crystallization temperature is indeed much higher than the T_gs of amorphous blocks (i.e. not a hard confinement for crystallization). The crystallization event is thus affected by other factors in addition to spatial confinement. As observed, the higher the sPS content the faster the crystallization rate. Consequently, we suggest that the growth rate of sPS in blends is strongly affected by the size of spherical microdomain (i.e. the confined effect in space) and the crossing-distance across the repulsive barrier of PEP matrix (i.e. the barrier for interconnection). For the blends having lower content of sPS (e.g. 15 wt% sPS content), the large crossing-distance for the interconnection of crystallization due to the remaining of HC matrix thus significantly obstructs the growth of crystallization. In the cases of higher content of sPS (e.g. 30 and 50 wt% sPS contents), the size effect of confinement becomes critical because of the approximately equivalent crossing-distance (Fig. 2b and c). As a result, the crystallization rate increases with increasing the added amount of sPS due to the increase in the size of spherical microdomain. Certainly, it is still immature to deal with the very complicated phase behavior and the crystallization under confinement in this study. Our aim is to provide appropriate interpretations for the observed crystallization behavior, and looking forward to explore the correlation between the changes on crystallization rates and the morphological observations.

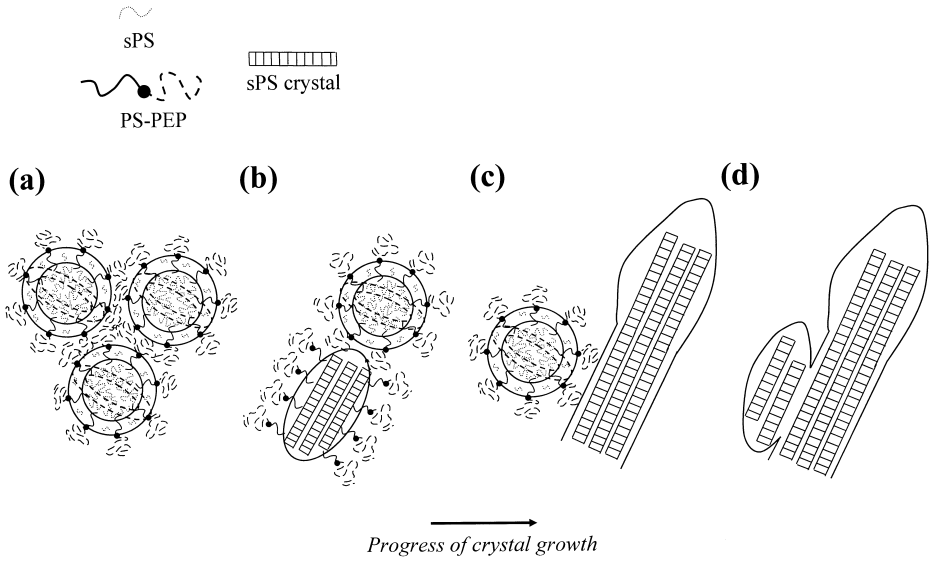

Fig. 10. Schematic diagram of crystal growth for sPS crystallized from the sPS/PS-PEP melt.

4. Conclusion

Self-assembly morphology, spherical microdomain texture with sPS embedded in PS-PEP matrix in the sPS/PS-PEP blends, was obtained by melt mixing. The crystallization behavior of the sPS in the blends was studied to attempt in understanding crystallization effect on morphological development. This study on the sPS crystallization from the core of the spherical microdomain (a physically confined system) provides experimental results for crystallization within a nano-confined environment without the effect of chemical connection. After crystallization, the morphology is transformed from initial spherical microdomain texture to crystalline domains. This suggests that the crystal growth overwhelms the confined effect in space and the repulsive barrier of immiscibility to form the final morphological state towards the minimum Gibbs free energy. The growth of sPS crystals was found being strongly dependent upon the size of spherical microdomain and the crossing-distance between the crystallizing sPS microdomains.

Acknowledgements

The financial support of the National Science Council (Grant NSC 90-2216-E-005 -010) is acknowledged. The authors thank Ms P.-C. Chao of Regional Instruments Center at NCHU for her help in TEM experiments. This work was carried out at NCHU and final writing was finished at NTHU.

References

[1] Mansky P, Chaikin PM, Thomas EL. J Mater Sci 1995;30:1987.
[2] Park M, Harrison C, Chaikin PM, Register RA, Adamson DH. Science 1997;276:1401.
[3] Huang E, Rockford L, Russell TP, Hawker CJ. Nature 1998;395:757.
[4] Bronstein L, Antonietti M, Valetsky P. In: Fendler JH, editor. Nanoparticles and nanostructured films: preparation, characterization and applications. New York: Wiley/VCH; 1998. p. 145.
[5] De Rosa C, Park C, Thomas EL, Lotz B. Nature 2000;405:433.
[6] Helfand E, Wasserman ZR. In: Goodman I, editor. Developments in block copolymers, Vol. 1. London: Applied Science; 1982.
[7] Bates FS, Fredrickson GH. Annu Rev Phys Chem 1990;41:525.
[8] Fredrickson GH, Bates FS. Annu Rev Mater Sci 1996;26:501.
[9] Hasegawa H, Hashimoto T. In: Aggarwal SL, Russo S, editors. Comprehensive polymer science. London: Pergamon; 1996.
[10] Hashimoto T. In: Holden G, Legge NR, Quirk RP, Schroeder HE, editors. Thermoplastic Elastomer. Munich: Hanser; 1996.
[11] Cohen RE, Cheng PL, Douzinas K, Kofinas P, Berney CV. Macromolecules 1990;23:324.
[12] Nojima S, Kato K, Yamamoto S, Ashida T. Macromolecules 1992;25:2237.
[13] Lovinger AJ, Han BJ, Padden FJ, Mirau PA. J Polym Sci Polym Phys 1993;31:115.
[14] Cohen RE, Bellare A, Drzewinski MA. Macromolecules 1994;27:2321.
[15] Rangarajan P, Register RA, Adamson DH, Fetters LJ, Bras W, Naylor S. Macromolecules 1995;28:1422.
[16] Ryan AJ, Hamley IW, Bras W, Bates FS. Macromolecules 1995;28:3860.
[17] Hamley IW, Fairclough JPA, Terrill NJ, Ryan AJ, Lipic PM, Bates FS. Macromolecules 1996;29:8835.
[18] Ryan AJ, Fairclough JPA, Hamley IW, Mai SM, Booth C. Macromolecules 1997;30:1723.
[19] Balsamo V, Stadler R. Macromolecules 1999;32:3994.
[20] Zhu L, Chen Y, Zhang A, Calhoun BH, Chun M, Quirk RP, Cheng SZD. Phys Rev B 1999;60:10022.
[21] Register RA, Loo YL, Adamson DH. Macromolecules 2000;33:8361.
[22] Hamley IW, editor. The physics of block copolymers. New York: Oxford University Press; 1998.
[23] Zhu L, Cheng SZD, Calhoun BH, Ge G, Quirk RP, Thomas EL, Hsiao BS, Yeh F, Lotz B. J Am Chem Soc 2000;122:5957.
[24] Park C, De Rosa C, Fetters LJ, Thomas EL. Macromolecules 2000;33:7931.
[25] Zhu L, Mimnaugh BR, Ge G, Quirk RP, Cheng SZD, Thomas EL, Lotz B, Hsiao BS, Yeh F, Liu L. Polymer 2001;42:9121.
[26] Loo YL, Register RA, Ryan AJ. Macromolecules 2002;35:2365.
[27] Ho RM, Chiang YW, Lin CC, Bai SJ. Macromolecules 2002;35:1299.
[28] Chien JCW, Salajka Z. J Polym Sci Polym Chem 1991;29:1253.
[29] Wunderlich B, editor. Thermal analysis. California: Academic Press; 1990.
[30] Hashimoto T, Tanaka H, Hasegawa H. Macromolecules 1990;23:4378.
[31] Tanaka H, Hasegawa H, Hashimoto T. Macromolecules 1991;24:240.
[32] Woo EM, Lee ML, Sun YS. Polymer 2000;41:883.
[33] Chang CC. M.S. Thesis, National Chung Hsing University; 2001.
[34] Jeon KJ, Roe RJ. Macromolecules 1994;27:2439.
[35] Shull KR, Winey KI. Macromolecules 1992;25:2637.
[36] Bodycomb J, Yamaguchi D, Hashimoto T. Macromolecules 2000;33:5187.
[37] Winey KI, Thomas EL, Fetters LJ. Macromolecules 1992;25:2645.
[38] Xie R, Li G, Liu C, Jiang B. Macromolecules 1996;29:4895.
[39] Lee SH, Char K, Kim G. Macromolecules 2000;33:7072.
[40] Hashimoto T, Koizumi S, Hasegawa H, Izumitani T, Hyde ST. Macromolecules 1992;25:1433.
[41] Spontak RJ, Smith SD, Ashraf A. Macromolecules 1993;26:5118.
[42] Winey KI, Thomas EL, Fetters LJ. Macromolecules 1992;25:422.
[43] Koizumi S, Hasegawa H, Hashimoto T. Macromolecules 1994;27:7893.
[44] Yamaguchi D, Shiratake S, Hashimoto T. Macromolecules 2000;33:8258.
[45] Mani S, Weiss RA, William CE, Hahn SF. Macromolecules 1999;32:3663.
[46] Loo YL, Register RA, Ryan AJ. Phys Rev Lett 2000;84:4120.
[47] Loo YL, Register RA, Ryan AJ, Dee DT. Macromolecules 2002;34:8968.
[48] Chen HL, Hsiao SC, Lin TL, Yamauchi K, Hasegawa H, Hashimoto T. Macromolecules 2001;34:671.